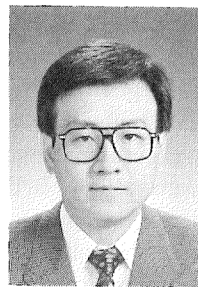


SHEAR RESISTANCE AND DUCTILITY OF RC COLUMNS AFTER YIELD OF MAIN REINFORCEMENT

(Translation from Proceedings of JSCE, No.585/V-38, February 1998)



Xuehui AN



Koichi MAEKAWA

During the Hanshin-Awaji Earthquake, catastrophic shear failure accompanying plenty of diagonal shear cracks was experienced in RC structures and bridge piers serving transportation facilities. In this paper, shear capacity and ductility of RC columns in the post-yield range of longitudinal reinforcement are discussed for seismic-resistant-design. First, the shear failure of large-scale RC columns is computationally simulated for an understanding of the mechanism of shear collapse of bridge piers. FEM computational results on ductility are compared with the experiments and a parametric study is conducted concerning factors that affect the post-yield deformability of RC columns. Finally, a simple formula for ductility is presented for summarizing the sensitivity of influential factors.

Keywords: shear failure, ductility, diagonal crack, RC column, FEM, size effect

Xuehui AN is an engineer at Tokyo Electric Power Services Co., Ltd.. He obtained his D. Eng. from the Univ. of Tokyo in 1996. He is a member of the JSCE.

Koichi MAEKAWA serves as a professor in the Dept. of Civil Engineering at the Univ. of Tokyo. He obtained his D. Eng. from the Univ. of Tokyo in 1985. He specializes in nonlinear mechanics and the constitutive laws of reinforced concrete, seismic analysis of structures, and concrete thermodynamics. He is a member of the JSCE and the JCI.

1. INTRODUCTION

Through the investigation of RC columns for bridge piers that failed in the Hanshin-Awaji Earthquake¹⁾, two kinds of typical damages were found to have occurred in columns with different dimensional features. For columns with a smaller section and a large span-to-depth ratio, large deformation is thought to follow the yielding of main reinforcement accompanying residual flexural crack opening (Fig. 1a). But no catastrophic collapse occurred in this kind of RC column. The columns were able to support the super structure and continued to serve as bridge piers. This is an important point in view of the maintaining transportation capabilities. The repair of RC columns damaged in flexural mode was not very difficult in practice.

The other kind of damage was unstable and brittle catastrophic shear failure. There are many RC piers with comparatively smaller shear span-to-depth ratio, larger sections, small main reinforcement ratios and much small web reinforcement ratios. After the earthquake, shear cracks were clearly observed in these columns (Fig. 1b). It seems that these RC columns with diagonal shear cracks lose their load-carrying capability immediately upon shear failure and suddenly stop acting as bridge piers. This kind of collapse is generally dangerous and should be avoided even in the case of strong earthquakes that exceed expectations. In this paper, the shear collapse mechanism and ductility of RC column in the post-yield range of reinforcement are discussed and numerically simulated for an understanding of the reduction in intrinsic shear capacity associated with deformation.

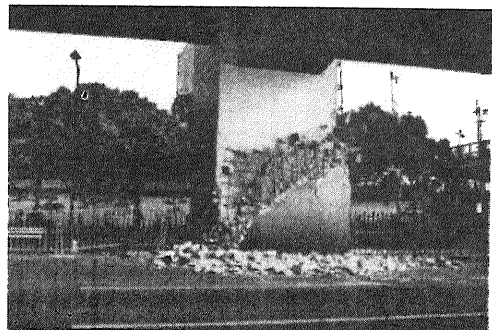
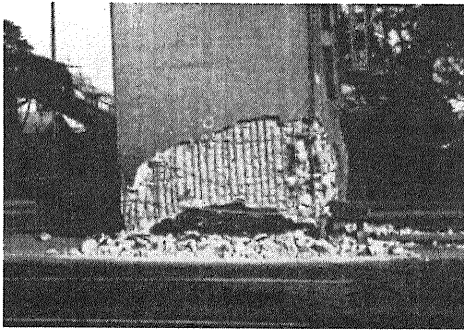


Fig. 1a Flexural damage after yielding of main reinforcement Fig. 1b Damaged column with diagonal shear cracking

2. NONLINEAR CONSTITUTIVE MODELS AND VERIFICATIONS

2.1 Constitutive models applied to RC columns

Constitutive models have been proposed for simulation of RC member behavior using the finite element method for engineering purposes²⁾, based on the smeared crack approach applied to finite control domains including distributed fixed multi-directional cracks. Here, all stress-strain relationships are indicated in terms of the spatial average stress and average strain of concrete as defined in finite elements. This chapter simply summarizes the model used in the shear analysis, since reference (2) offers full details.

a) Cracked concrete model in RC zone³⁾

The reinforced concrete model is constructed by combining the constitutive law for concrete and that for reinforcing bars (Fig. 2). The constitutive law adopted for the cracked concrete consists of tension stiffness, compression, and shear transfer models.

Once cracks are generated in the concrete, anisotropy becomes significant, so the stress-strain relationship takes on an orthogonal anisotropy along the crack direction. The stress-strain relations are modeled by being decomposed in directions parallel to, along and normal to cracks, respectively.

Owing to bonding action between concrete and reinforcing bars, the concrete continues to support some of the tensile force even after dispersed cracks occur in reinforced concrete zones. To take into account the effects of bond on RC deformation, the relation between average stress and average strain of concrete is given as a macroscopic tension model for cracked concrete. This tension model mechanically describes how the tensile stress is transferred from steel bars to the concrete beyond the cracks by bond.

This constitutive law for reinforced concrete, which derives from a control volume consisting of a 30-50 cm sized concrete element with distributed cracks, is independent of crack spacing owing to the trade-off mechanism between bond deterioration zones and their developed length⁵⁾. It is verified that in the case of normal concrete and two-way reinforcement with a ratio over 0.1% to 2%, this constitutive law is independent of the size of the control volume, unlike the plain concrete case. This cracked concrete model is rather simple, as the mean behavior of cracked concrete is unrelated to the crack spacing, the orientation of reinforcing bars, and reinforcement ratio and has no size sensitivity⁵⁾.

The shear transfer model of cracked concrete in RC is based on the contact density idealization⁶⁾.

It was mathematically and experimentally proved that the shear stiffness of the cracked concrete zone is not affected by the crack spacing and density^{3), 5)}. This means there is an element-size insensitivity of shear behavior along cracks in RC zones.

b) Effective size of RC zone

We cannot expect a mean stress transfer via bonding around certain parts which contain no reinforcement and which are not reached by the tension stiffness mechanism. It is proposed to separate the whole structural volume into RC zone and plain one and the effective size of RC zone was discussed as one of influential factors for size effect computation²⁾. The size of the RC zone in the analysis domain has an effect not only on the stiffness of a member after cracking, but also on the failure mode, which may change from shear to flexure as the size of the RC zone increases. The mechanical features of reinforced/plain concrete zoning as they relate to the volume of crack propagation stability was investigated by the authors with respect to the size effect in the shear capacity of RC members before yielding of the longitudinal reinforcement²⁾. This paper aims at the same discussion in view of the post-yield behavior of RC members in shear.

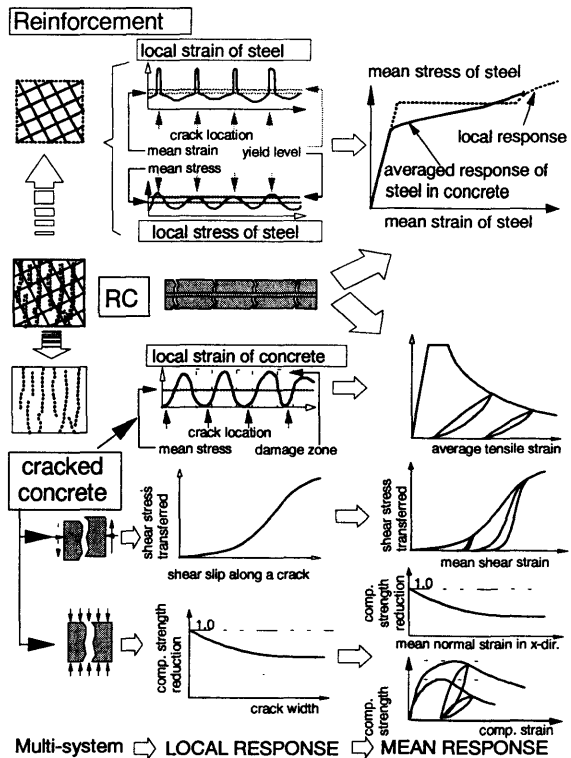


Fig. 2 Cracked concrete model in RC zone⁴⁾

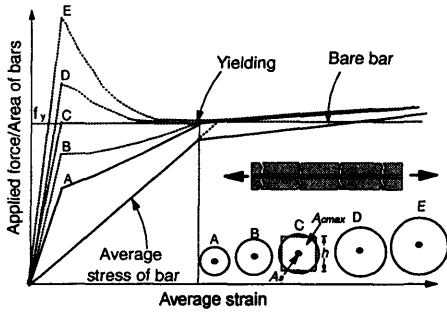


Fig. 3 Crack control capability and concrete area

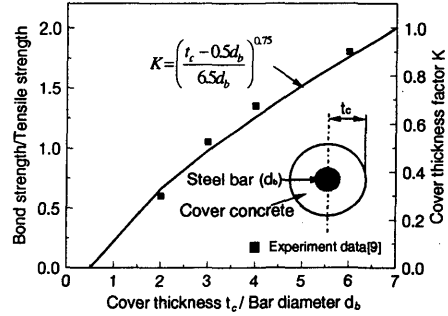


Fig. 4 Cover effect on bond strength and factor K

We propose that size of the RC zone is associated with the tension stress transfer mechanism resulting from bonding characteristics, as mentioned in the previous section. In the critical case as shown in Fig.3, if a reinforced concrete member subjected to tension contains a small amount of reinforcement, the reinforcing bars crossing the crack may yield just after cracking and most inelastic deformation will be rooted in the sole crack. This is a critical issue can adequate crack control be assured when there are several cracks be obtained. For a certain steel bar, the maximum size of the reinforced concrete zone within which stable cracks can develop is,

$$A_{cmax} = \frac{A_s \cdot f_y}{f_t} \quad (1)$$

where, A_s : area of steel bar, A_{cmax} : maximum area of bond effective zone in concrete, f_y : yielding strength of steel bar. In a two-dimensional computation²⁾, it was proposed using the relation for RC zone depth given in Fig.3 and the following steel bar diameter:

$$h_{max} = \frac{\sqrt{\pi}}{2} \cdot d_b \cdot \sqrt{\frac{f_y}{f_t}} \quad (2)$$

where, h_{max} is the depth of the RC zone and we have $A_{cmax} = h_{max}^2$, d_b as the diameter of reinforcing bar.

This formula describes the case where the concrete cover is thick enough to avoid splitting failure⁷⁾. If not, the ability of a deformed bar to transfer its load into the surrounding concrete is considerably limited by splitting along the bar axis. Experimental studies to confirm the effects of cover on longitudinal splitting crack formation have been conducted⁸⁾. Some results of the relation between bond strength and specific cover are shown in Fig.4. Bond capacity decreases as the concrete cover is reduced. When there is insufficient cover, we propose that the formula in Eq.(2) to be factorized by an empirical function K based on these test results²⁾,

$$K = \left(\frac{t_c - 0.5d_b}{6.5d_b} \right)^{0.75} \quad (3)$$

where, K: modification factor for cover thickness, ($K=0$ when $t_c < 0.5d_b$ and $K=1$ when $t_c > 7d_b$) and t_c : thickness of concrete cover.

In two-dimensional finite element computations, the depth of the RC zone for steel bars with a wide variety of arrangements must be determined. The proposed basic rule²⁾ is that the depth of the RC zone is determined by the diameter of each bar. If bars of larger diameter are used, the RC zone becomes larger (Fig.5a).

Another extreme case to be considered is when the steel bars are placed at a great distance from each other. The size of the RC zone may then be smaller than that computed by Eq.(2), as the steel bars

cannot control the crack distribution in the whole volume of concrete between them (**Fig.5b**). Thus, the depth of RC zone used in computation was proposed as,

$$h_e = \frac{n \cdot h_{max}^2}{b} \quad (4)$$

where, h_e : modified depth of RC zone, n : number of steel bars, b : thickness of RC member.

When the bars are very small or placed far apart, a situation where one element contains both RC and plain concrete (PL) zones must be considered. The stress-strain curve of this element with mixed zones can be decided by solving Eq.(5), the fracture energy balance²⁾, in terms of c_m as,

$$\int_0^{\infty} \sigma_t(\epsilon_t; c_m) d\epsilon_t = \frac{(l_e - h_e) \int_0^{\infty} \sigma_{PL} d\epsilon_t + h_e \int_0^{\infty} \sigma_{RC} d\epsilon_t}{l_e} \quad (5)$$

where, $\sigma_{RC} = \sigma_t(\epsilon_t; 0.4 \vee 0.2)$ in Eq.(2) and $\sigma_{PL} = \sigma_t(\epsilon_t; c_{pl})$ in which c_{pl} is defined later; and l_e : height of the finite element.

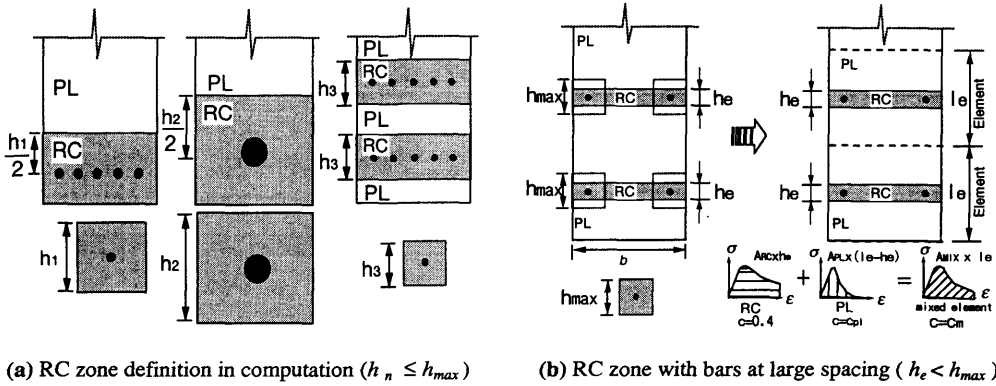


Fig. 5 RC zoning method

c) Cracked concrete model in PL zone

Cracked plain concrete shows strain-softening characteristics in tension and shear, unlike concrete confined by reinforcing bars. Here, the mean stress-strain relation turns out to be element-size dependent and is formulated with respect to the fracture energy⁹⁾. Based on the fracture energy balance, the average stress-strain curve defined in an element is adjusted according to the reference length l , which is the square root of the element area as shown in Fig.6.

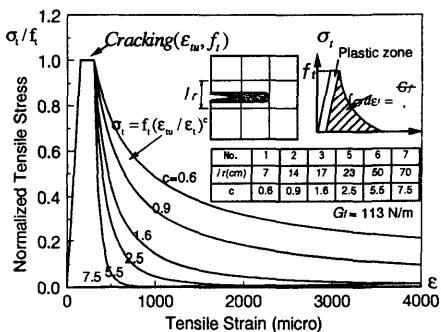


Fig. 6 Tension stress-strain softening in computation

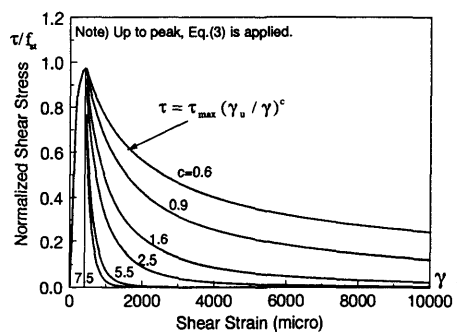


Fig. 7 Shear stress-strain softening for plain concrete (tensile strain = 0.00005; ultimate shear strain $\gamma_u = 0.0004$)

In the model proposed by the authors²⁾, the tension factor denoted by “c” is inversely related to the element size such that fracture energy remains constant. Figure 6 gives the series of tensile stress-strain curves used for the following analysis. Here we use the same reason for shear mode. The Bujadham model²⁶⁾ describes contact softening in shear transfer. A simplified softening model which is equivalent to the original one is proposed, that is, when the shear strain reaches the ultimate value, shear softening begins (Fig.7). Since the shear transfer mechanism is highly frictional, no unique shear softening energy is available, rather it is dependent on the confinement normal to the cracks. The proposed model of crack shear is also developed as a combination of the cracked concrete models in the RC zone and PL zone, based on the RC zoning method.

2.2 Verification of proposed models

The FEM code **WCOMD-SJ**, in which the proposed models are installed, provides computations for size effect experiments⁴⁾ as shown in **Fig. 8**. This size effect experiment consists of large RC beams without shear reinforcement and with different effective depth from 10cm to 300cm. The specified properties are listed in **Table 1**. The main reinforcement ratio in the vicinity of the support points, where shear failure is designed to occur, is taken to be 0.4%. The beams are loaded by uniformly distributed hydraulic pressure until failure. The observed failure modes are flexural failure for beams No.1,2 and shear failure for the other beams.

The shear strength estimated by the equation¹⁰⁾ given in JSCE code is also shown in **Fig. 8** for comparison. It can be seen that the proposed model predicts the shear strength with the size effect and has fair agreement with the JSCE code. The crack pattern in **Fig. 8** also shows that the computation can simulate the crack development and failure mode correctly²⁾.

For verification with respect to reinforcement ratio ρ and compressive strength f_c' , computational results for beams with varying ρ and f_c' are plotted in **Fig. 9**. The predicted shear strength is proportional to $\rho^{1/3}$ and $f_c'^{1/3}$, similar to the sensitivity of the JSCE equation. Since the JSCE shear strength equation is capable of predicting the actual behavior within a 10% coefficient of variation, it may be used for indirect experimental verification of the FEM computations.

Table 1 Specified properties of RC beams⁴⁾

	Depth	Concrete strength	Shear Strength	Shear Strength
	d	f_c'	Exp.	Comp.
	cm	kgf/cm ²	kgf/cm ²	kgf/cm ²
1	10	202	(7.38)	(6.75)
2	20	193	(8.41)	(7.02)
3	60	207	4.55	4.59
5	100	215	3.87	4.05
6	200	279	3.40	3.51
7	300	240	3.09	3.24

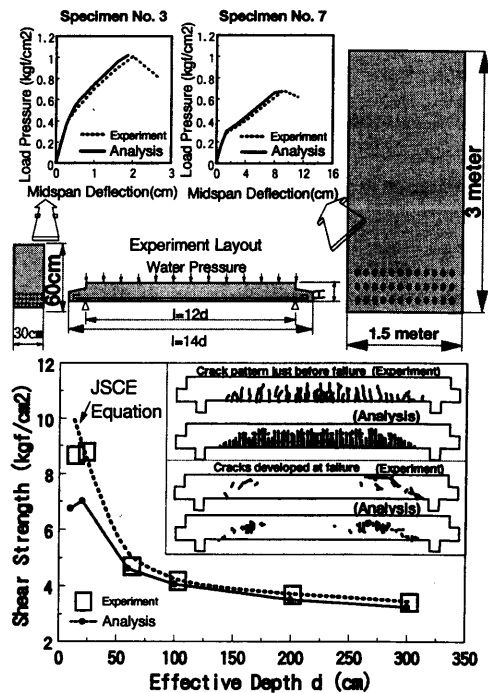


Fig. 8 Computational results and size effect oriented experiments²⁾

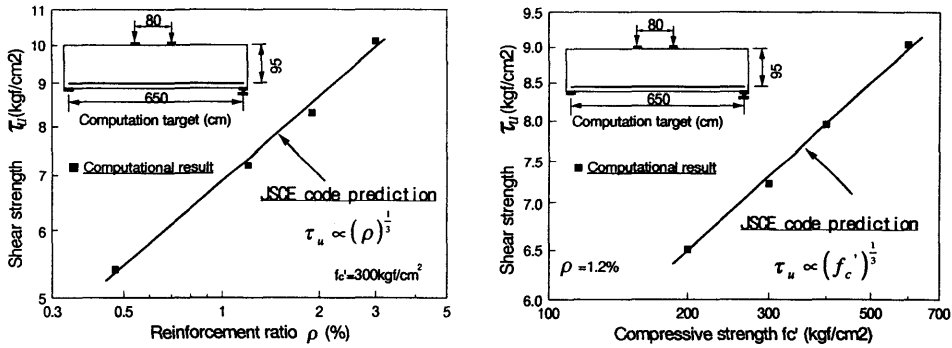


Fig. 9 Effect of reinforcement ratio and concrete compressive strength on nominal shear strength

2.3 Nonlinear characteristics of concrete partly confined by web reinforcement

As discussed in the previous section, concrete in RC zone exhibits different post-cracking nonlinearity from place to place in both tension and shear, and shows brittleness when located apart from reinforcement. To deal with cracked concrete in different parts of structures, the proposed models in section (1) are adopted in studying larger-scale RC columns, too.

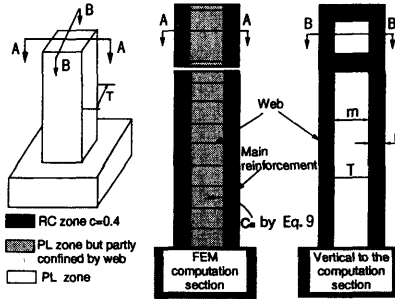


Fig. 10 Zoning for RC column with little web reinforcement

In considering large-scale RC columns with web reinforcement, the three-dimensional arrangement of web bars must be considered. Its mechanical conversion to two-dimensional analysis is shown in Fig. 10. In section 2.1, a mixed element was proposed for FEM elements including both RC and plain zones, aiming to simulate the effect of well-separated longitudinal steel bars in beam analysis. Here, the authors adopt a similar concept for web portions including lateral bars with large spacing (Fig. 10).

Let n and m denote, respectively, the thickness of the RC skin layer created by web reinforcement, as shown in Fig. 10, and the size of the plain core of the column in the thickness direction of a 2D projection. The diagonal shear crack-based energy release is expected to be the sum of the energy absorb by both the RC skin layers and the plain volume. Then, similar to Eq.(5), we can have a fracture energy conservation as,

$$\int_0^{\infty} \sigma_t(\varepsilon_t; c_m) d\varepsilon_t = \frac{m \int_0^{\infty} \sigma_{PL} d\varepsilon_t + n \int_0^{\infty} \sigma_{RC} d\varepsilon_t}{(n+m)} \quad (6)$$

By solving Eq.(6), we obtain c_m for the elements allocated to the web zones of the columns concerned.

An existing RC bridge pier is selected for verification. It has a 2m×2m square section with a main reinforcement ratio of 0.4% and a web ratio of 0.05%. The computational result is shown in Fig. 11. The computed nominal shear capacity is 5.3kgf/cm². From Fig. 11b, the shear crack band at the last unstable failure step is identical. According to the JSCE code, the estimated shear strength of this column is 5.2kgf/cm². The FEM simulation has reasonable agreement with the JSCE prediction.

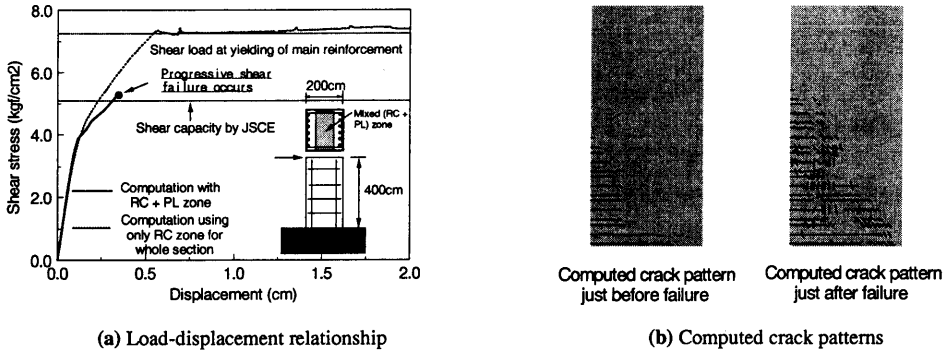


Fig. 11 Shear failure of RC column with web reinforcements

3. FAILURE MODE AND DUCTILITY PREDICTION OF RC COLUMNS

Table 2 Experiments of shear mode failure after yielding of longitudinal reinforcement

Series No.	1	1	1	2	2	3
Ref.	[11]	[11]	[11]	[12]	[12]	[12]
Width B (cm)	80	80	80	40	40	40
Effective depth d (cm)	35	35	35	35	35	35
Shear span to depth ratio a/d	4.0	4.0	4.0	4.0	4.0	4.0
Axial stress (kgf/cm ²)	10	10	10	10	10	0
Main reinforcement ratio (%)	0.86	0.86	0.86	1.66	1.66	2.48
Web reinforcement ratio (%)	0.08	0.16	0.04	0.27	0.42	0.58
V_c (kgf/cm ²)	7.7	7.7	7.7	9.8	9.8	11.2
V_s (kgf/cm ²)	2.1	4.2	1.1	7.9	12.3	20.2
P_y (kgf/cm ²)	7.9	7.9	7.9	15.5	15.5	21.4
$(V_c+V_s) / P_y$	1.30	1.53	1.14	1.23	1.56	1.46
μ (By test)	3.9	4.2	3.0	5.0	7.0	5.9
μ (By FEM)	3.8	4.0	3.2	4.9	5.8	5.5
Failure mode	shear	shear	shear	shear	shear	shear

Note: V_c : shear carrying capacity of concrete evaluated based on JSCE specification; V_s : shear carrying capacity of web steel based on yielding (JSCE specification); P_y : shear force at which yielding of main reinforcement occurs; μ : ductility ratio ($=\delta_u/\delta_y$; δ_u : ultimate displacement when diagonal shear failure occurs; δ_y , yield displacement) See Eq.(11)

It is well known that the ductility of an RC column is associated with its shear carrying capacity. Normally, an increase in web reinforcement raises the higher ductility of a column, as is clearly shown by experiments^{(11),(12)}. Here, three experiments based on FEM simulations are reported. The first and

second cases are with joint elements placed between footing and columns. The third one is a reinforced concrete column with side reinforcement.

The experimental details are shown in **Table 2**. The calculated shear capacities are listed in the table according to the JSCE code prediction, and are larger than the shear force when yielding of main reinforcement occurs. Thus, brittle shear failure before yielding is avoided. However the shear carrying capacity of each specimen is not so high as to exceed twice the shear force at yield. According to criteria newly proposed by the JSCE¹³⁾, these specimens would be expected to fail in shear mode after yielding of the main reinforcement.

The FEM simulation of ductility associated with shear failure is verified using the test data. **Fig. 12** shows the target of the verification from Ref.[11], and **Fig. 16** that from Ref.[12]. The computed results are shown in **Fig.13** and **Fig.17**, respectively. The computational loop stops at the point where the shear strain increases sharply and becomes larger than a critical value (set as 1% in this work). The displacement at this point is taken as the ultimate value, while the ductility at this point is used for comparison with that at the point of maximum load in the experimental loop, which continues after the load peak and then becomes smaller and smaller. It can be seen that FEM computed results have fair agreement with experimental ones. Both the experimental and computational results indicate that an increase in web reinforcement ratio in the RC column yields higher ductility. In order to confirm the failure mode in the computation, the crack pattern for a specimen is shown in **Fig. 14**, in comparison with the observed shear cracks in the experiment. A diagonal crack pattern is seen in both experiment and analysis.

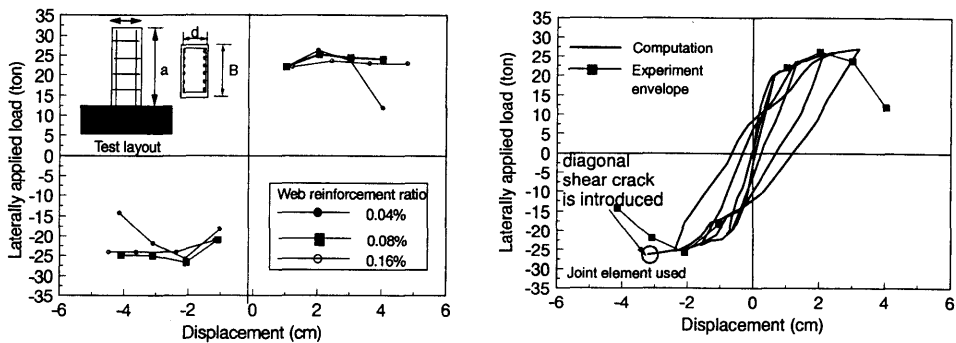
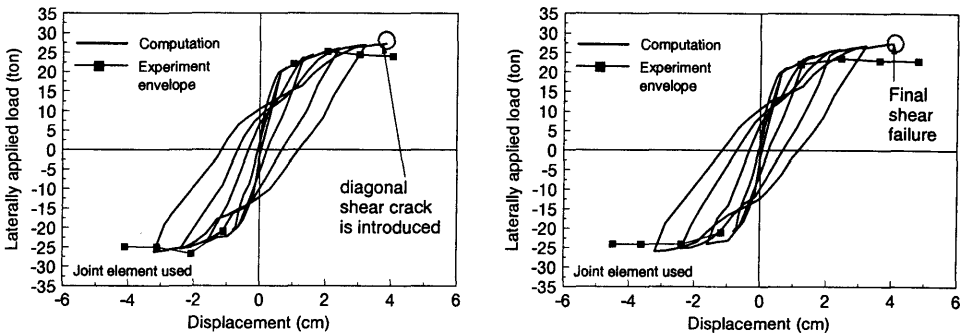


Fig. 12 Envelope of cyclic load-displacement relation of RC columns¹¹⁾ (a) Web reinforcement ratio= 0.04%



(b) Web reinforcement ratio = 0.08%

(c) Web reinforcement ratio=0.16%

Fig. 13 Computed ductility and hysteresis response

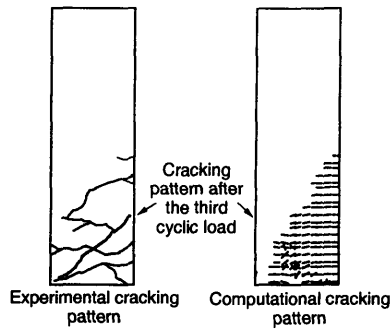


Fig. 14 Crack pattern comparison at shear failure (web reinforcement ratio = 0.08%)

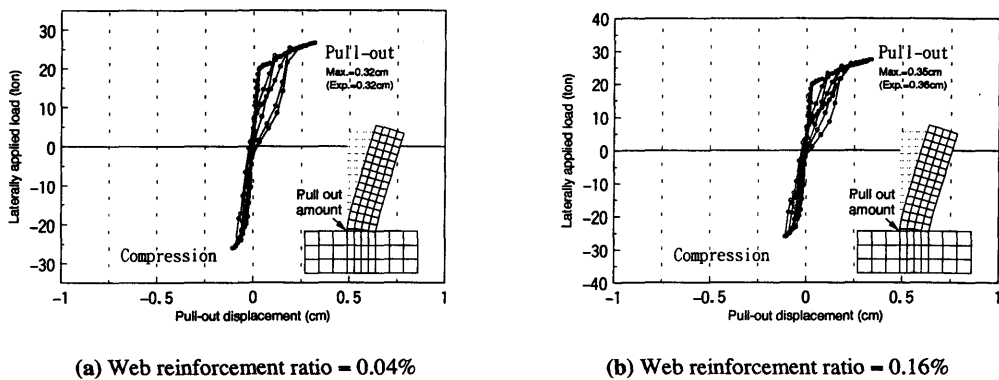


Fig. 15 Pull-out displacement from computation

In order to confirm the behavior of the joint element, the computed pull-out displacement for Case 1 is compared with the observed data in Fig.15. The total displacement increases by about 30% because of this pull-out effect.

The FEM simulation for an RC column with side reinforcement¹²⁾ under monotonic loading is shown in Fig. 18. It is reported that side reinforcement raises shear carrying capacity prior to yielding of main steel bar¹⁸⁾. The ductility of RC columns with side reinforcement after yielding of the main reinforcement can also be simulated by FEM computation. All these results support the hypothesis that the shear failure and the ductility level of RC columns after yielding of the main reinforcement can be estimated by FEM analysis proposed in Chapter 2.

In all experiments, the sectional size is less than 1 meter. In this section, the shear failure before longitudinal reinforcement yielding in a 2m × 2m RC column is simulated by FEM. In order to check the effect of web reinforcement on failure mode and ductility, additional web reinforcement is used in the reference case for sensitivity analysis as listed in Table 3. The failure mode changes according to the web reinforcement ratio as calculated in Table 3. First, the web reinforcement ratio is specified 0.15%. The total shear capacity is higher than the shear load when yielding occurs but the shear carrying capacity estimated by the JSCE code is much smaller than twice the shear load when yielding occurs. Thus, the column may fail in shear mode after yielding of main longitudinal reinforcement, resulting in less ductility.

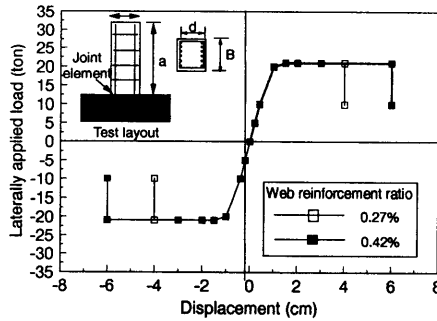
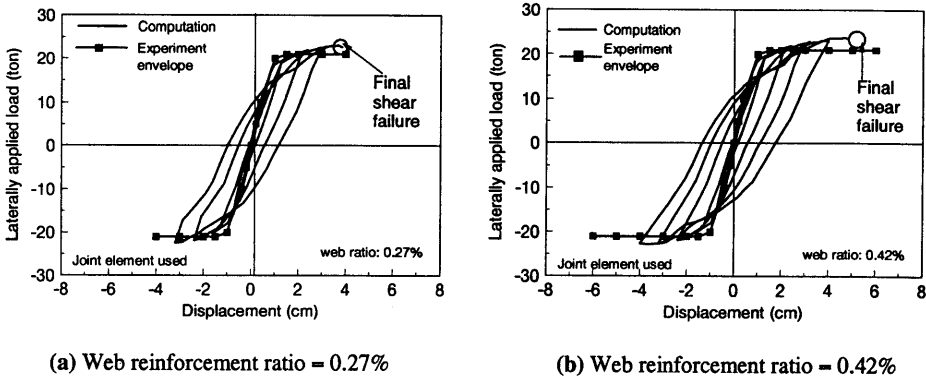


Fig. 16 Envelope of cyclic load-displacement relation of RC columns with different web ratios¹²⁾



(a) Web reinforcement ratio = 0.27%

(b) Web reinforcement ratio = 0.42%

Fig. 17 FEM simulation concerning the effect of web ratio on ductility

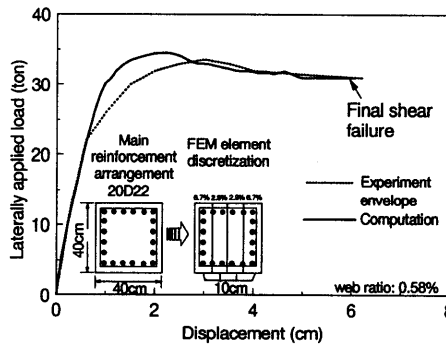


Fig. 18 FEM simulation for specimen with side reinforcement¹²⁾

If the web reinforcement is increased to 0.2% by volume, the shear capacity is increased but is still lower than two times the shear force at yield. Then, this case still brings shear failure, but higher ductility ratio can be expected. When the web reinforcement is increased to 0.35%, the shear capacity exceeds two times the shear force at yield. In this case, brittle shear failure may be avoidable and the RC column may fail in flexure with high ductility.

All these cases are simulated using nonlinear FEM as proposed in Chapter 2. The analytical results under monotonic loading are shown in Fig. 19. The failure mode is shown in the same figure with respect to the crack patterns at the last computational step; that is, the unstable failure point

where progressive cracking occurs in the iterative computation²⁾. From the crack patterns, it can be seen that the RC columns No.2 and No.3 fail in shear mode after yielding of main bars, but for No.4, the computation terminates in compression failure of the concrete at the extreme fiber closest to the maximum moment section.

Table 3 Failure mode prediction for large-scale RC columns

No.	1	2	3	4
Width B (cm)	200	200	200	200
Effective depth d (cm)	190	190	190	190
Shear span a/d	2.0	2.0	2.0	2.0
Main reinforcement ratio (%)	0.4	0.4	0.4	0.4
Web reinforcement ratio (%)	0.05	0.15	0.20	0.35
V_c (kgf/cm ²)	3.9	3.9	3.9	3.9
V_s (kgf/cm ²)	1.5	4.5	6.0	10.5
P_y (kgf/cm ²)	7.0	7.0	7.0	7.0
$(V_c+V_s) / P_y$	0.8	1.2	1.4	2.1
μ (By FEM)	<1.0	2.4	4.8	13.2

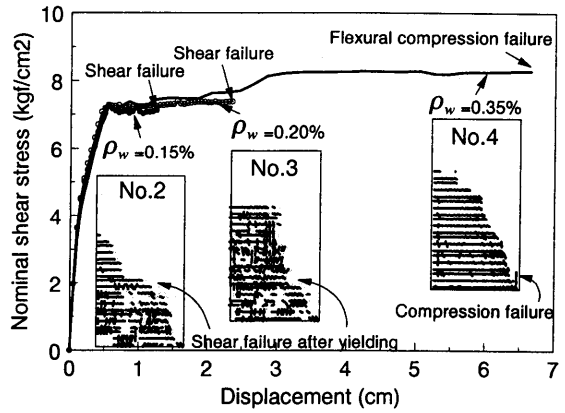
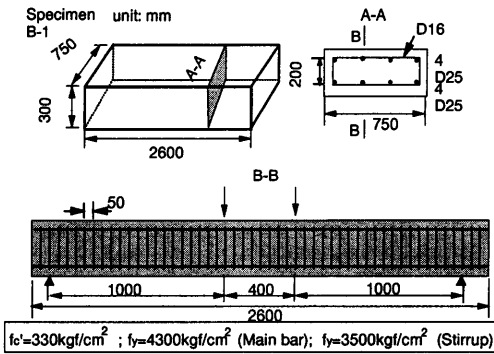
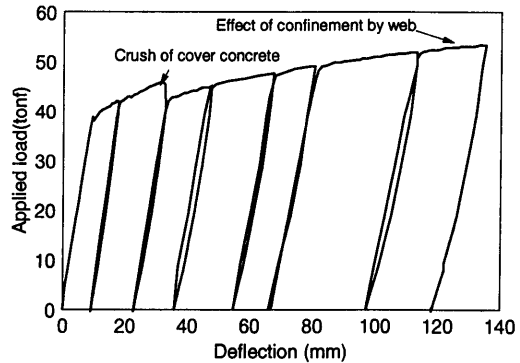


Fig. 19 Effect of web reinforcement ratio on ductility of large scale RC column in computation

If the RC column is heavily reinforced with web steel and the concrete is well confined by the web reinforcement, compression failure of the concrete is almost non-existent. **Fig. 20a** shows an RC beam with a high web reinforcement ratio of 1%. Here, the core concrete is fairly well confined. The experimental result shows that only the cover concrete is crushed, but the test can continue without further compression failure of the core concrete (**Fig. 20b**).



(a) Experimental layout with heavy web (1%)



(b) High ductility level in the case large web reinforcement ratio (1%)

Fig. 20 Experimental result for RC beam with high ductility level

4. PARAMETRIC STUDY ON DUCTILITY OF RC COLUMNS

As described in the previous section, the FEM analysis method may be used to estimate the ductility of RC columns with reasonable accuracy when the failure mode is shear. Now, FEM analysis is used for a parametric study on factors that influence deformability. In the computation, no iteration is carried out in each cyclic load step and spalling is not yet included in the constitutive model of RC. The main factors relating to ductility are empirically known; that is, the main and web reinforcement ratios, axial force, and shear span-to-depth ratio (a/d) of the column. The sensitivity of these factors can be numerically examined, and some experimental results²⁴⁾ will be employed to reverse check for versatility. The ranges of the parameters discussed are shown in Table 4.

Table 4 Ranges of parameters that affect ductility

Parameter	FEM	Test [24]
Main reinf. ratio (%)	0.9-2.1	0.89-1.66
Web reinf. ratio(%)	0.08--0.36	0.08--0.23
Axial comp. stress(kgf/cm ²)	0--20	0-20
a/d	3-6	3-6

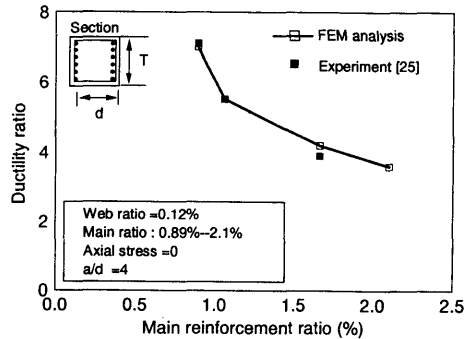


Fig. 21 Effect of main reinforcement ratio on ductility

All the computations are carried out under monotonic loading. Details of computational targets and the results are shown in Fig. 21 to Fig. 24. In computing the ductility factor, the definition of yield displacement is rather different among technical reports and there is vagueness regarding sections with side reinforcement. Within the scope of this study, the authors intentionally select specimens without side reinforcement. In this case, the definition of yield displacement as when bars start to yield is quite explicit, because the main reinforcement becomes plastic at the same time under flexure. We can then consistently adopt the experimentally reported ductility from different investigators. From these results, some tendencies are clearly identified as follows.

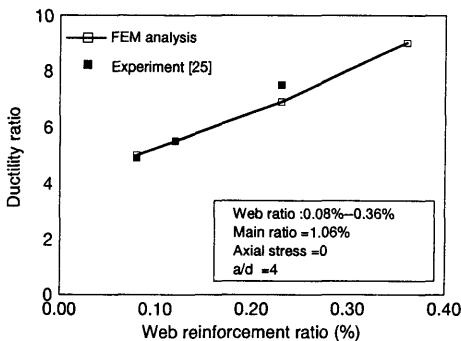


Fig. 22 Effect of web reinforcement ratio on ductility

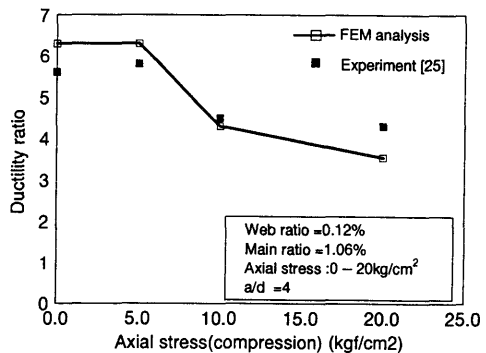


Fig. 23 Effect of axial stress on ductility

- As the main reinforcement ratio increases, ductility decreases.
- An increase in web reinforcement ratio elevates the ductility of RC columns.
- The ductility tends to decrease when higher axial compressive force is applied.
- As the shear span to depth (a/d) ratio increases, the ductility also increases.

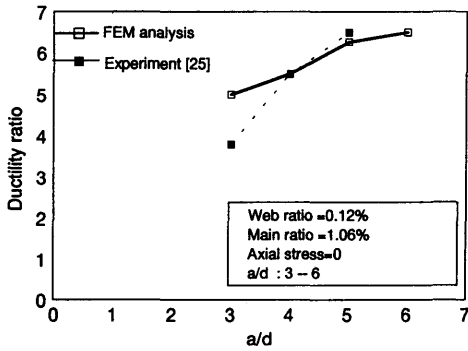


Fig. 24 Effect of a/d on ductility

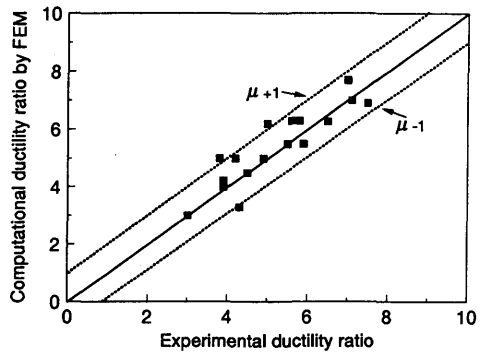
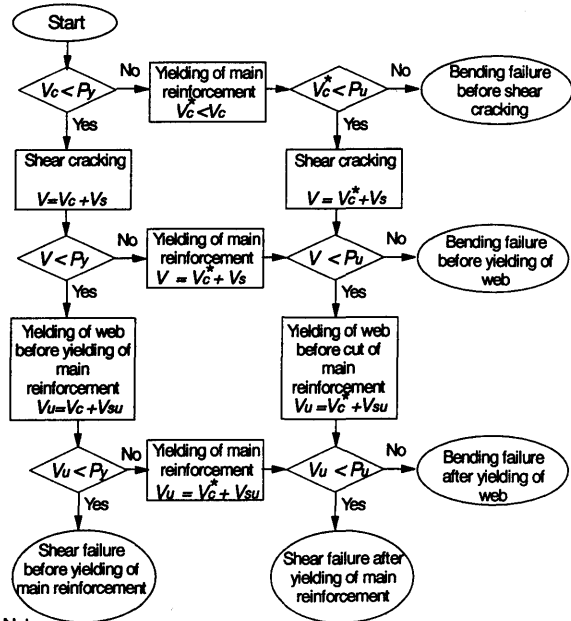


Fig. 25 Ductility ratio comparison^{(11), (12), (24)}

Computed ductility ratios are summarized in Fig.25, in comparison with experimental results. It can be seen that the FEM simulation may give good predictions. The ductility associated with flexural action is outside the scope of this study, and further research on the buckling of bars and spalling of cover concrete will be needed.



Note:
 V_c : Shear capacity carried by concrete
 V_s : Shear capacity carried by web based on yielding strength
 V_{su} : Shear capacity carried by web based on ultimate strength
 V_c^* : Decreased shear carrying capability of concrete after yield of main bars
 V : Shear capacity RC member based on yielding of web
 V_u : Ultimate shear capacity of RC member
 P_y : Shear force at yielding of main reinforcement
 P_u : Shear force at ultimate strength of main reinforcement

Fig. 26 Failure mode check-flowchart for RC column

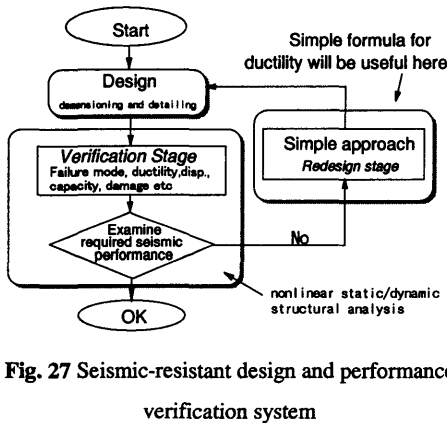


Fig. 27 Seismic-resistant design and performance verification system

5. SIMPLIFIED CHECK METHOD FOR FAILURE MODE

5.1 General

It has been determined that nonlinear response of RC linear members can be traced up to unstable shear failure before and after yielding of the longitudinal reinforcement. Consequently, the computed overall response to seismic motions can form the basis for examining the required seismic performances. Fig. 27 shows a possible flowchart for seismic performance evaluation. In this scheme, nonlinear dynamic FEM analysis plays a substantial role by simulating the nonlinear behavior on which the seismic performance is verified.

If planned structural dimensioning and detailing are not accepted after checking the performance, some or all of the design decisions on which the decision was made at the design stage have to be modified (the re-design stage in Fig. 26). At this stage, simple but reasonably accurate formula would be useful for practitioners who have to find solutions which satisfy the performance requirements.

In the re-design stage, a prompt judgment on the failure mode of RC members is valuable. A proposal for identifying the inherent failure mode of members is shown in Fig. 26. If the estimated shear capacity is larger than the shear force when the main reinforcement yields, shear failure before yielding can be avoided. Much research^{14,15} has shown that shear failure occurs even after yielding of the steel occurs. It is now understood that the shear carrying capacity of concrete may decrease after plastic deformation of main reinforcement^{16,17}. As a result, shear failure after yielding may occur if the reduced decreased shear capacity is below the ultimate load corresponding to the ultimate strength of the main reinforcement, as shown in Fig. 28. This kind of failure mode is also unwanted, since rather brittle failure with small displacement accompanies it.

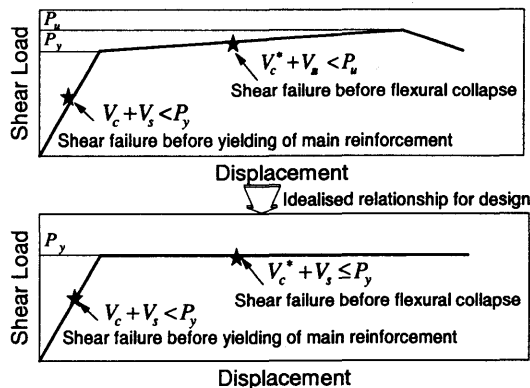


Fig. 28 Idealized shear load-displacement relationship of RC column

In this section, a simple evaluation of shear capacity in the post-yield range is sought. In the previous chapter, the predicted ductility was found to be close to reality, and the factors influencing were clearly identified for sections without side reinforcement, within which the authors limited the scope of their discussions. In this discussion, the analytically obtained sensitivity will be used to form a degenerated simple formula with a re-design orientation in the scheme of seismic performance design.

5.2 Shear failure after yielding of main reinforcement

The shear capacity at the point when yielding of the web reinforcement occurs can be formulated as the sum of the shear force carried by the concrete and that carried by the web reinforcement. We thus have,

$$V = V_c + V_s \quad (7)$$

where, V : total shear capacity of a RC member (yield capacity of web reinforcement); V_c : shear carrying capacity of concrete; and V_s : shear carrying capacity of web steel based on yield.

If the shear capacity is larger than the shear force when yielding begins, shear failure prior to yielding can be avoided. Here, we have,

$$V > P_y \quad (8)$$

where, P_y : shear force that brings about yielding of longitudinal reinforcement.

As the shear force carried by the concrete may fall after the main reinforcement reaches the plasticity limit, the post-yield shear capacity can be formulated as,

$$V = V_c^* + V_s \quad (9)$$

where, V_c^* : reduced shear carrying capacity of concrete.

The reduction in shear capacity related to deformation and crack propagation is indirectly taken into account by including the reinforcement ratio in the code equations when the pre-yield shear failure of RC beams is discussed. Similarly, the shear carrying capacity of concrete decreases after yielding of main reinforcement and the total shear potential also decreases. This may result in a capacity lower than the applied shear force, and finally cause lower ductility. The decrease in shear carrying capacity of concrete is an important factor that affects the deformational behavior of RC columns.

Reference [17] discusses the shear force carried by concrete and web steel. For several RC columns, the relation between total shear force and averaged stress in web steel was recorded and the shear force carried by the web and concrete was investigated as shown in Fig. 29.

It can be seen in Fig. 29 that the shear stress in the web increases as the shear force rises. And the shear force carried by the concrete remains almost constant before the main reinforcement yields. But after yielding of the main reinforcement ($\mu=1$; μ is defined as the ductility index), the shear becomes smaller and smaller as the shear stress in web continues rise. This phenomenon can be explained by a decrease in the shear force carried by the concrete after the main reinforcement becomes plastic. This decrease is also shown in Fig. 30.

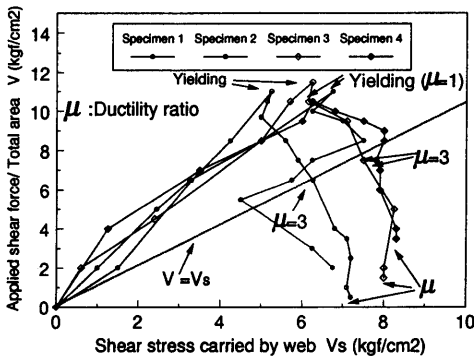


Fig. 29 Shear stress carried by web reinforcement experimental¹⁷⁾

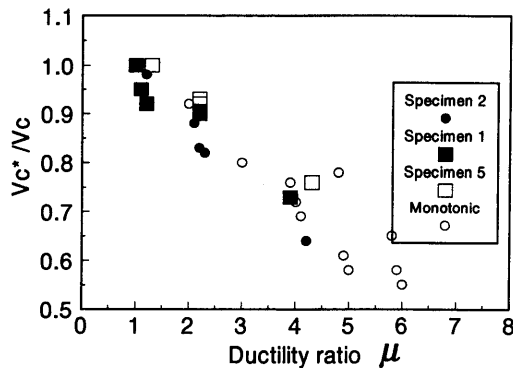


Fig. 30 Decrease in shear force carried by concrete after yielding of main reinforcement from experiments¹⁷⁾

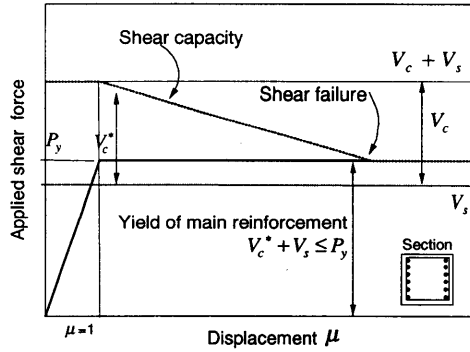


Fig. 31 Mechanism of shear failure after yielding of main reinforcement

Based on this understanding that the shear capacity falls off, the post-yield shear failure mechanism can be described as illustrated in Fig.31. As the shear carrying mechanism is not fully understood, a quantitative analytical approach is useful for describing the decrease in nominal shear force carried by the concrete.

In order to discern this decrease in the shear capacity of concrete, about 200 experimental data points for RC columns references [15,18,19,20,21,22,23, and 24] were checked of these 53 specimens failed in post-yield shear failure mode. These specimens had main reinforcement ratios varies from 0.51% to 1.89%, web reinforcement ratio from 0 to 0.23%, axial compression stress from 0 to 30kgf/cm², and shear span-to-depth ratios from 3 to 6. Since all specimens were square sections without side reinforcement, the yield forces can be clearly calculated and were easily determined from the experiments. Here, two definitions of ultimate deformation may be used, one is to take the deformation corresponding to 80% of the maximum load after peak as the ultimate value, and the other way is to indicate the deformation when the load decreases to the initial yield load after the peak. Reference [24] shows that these two definition lead to similar results when there is no side reinforcement.

From Fig.31, it can be shown that the lower shear capacity is close to the shear load at the yield point when shear failure takes place. Thus the reduced shear carrying capacity of concrete at shear failure can be inversely calculated by,

$$V_c^* = P_y - V_s \quad (10)$$

This loss in shear capacity may be affected by several factors, such as the reinforcement arrangement, the shear span-to-depth ratio, the axial force, and the concrete strength. All these factors also influence the ductility ratio of RC columns. The ductility ratio is generally defined as,

$$\mu = \frac{\delta_u}{\delta_y} \quad (11)$$

where, μ : ductility ratio; δ_y : displacement at yield point of main reinforcement; and δ_u : ultimate displacement when unstable diagonal crack propagation occurs.

The JSCE code gives the formula for shear capacity carried by concrete as,

$$V_c = 0.9\beta_p(\rho_t) \cdot \beta_2(f_c') \cdot \beta_d(d) \quad (12)$$

where ρ_t is the main reinforcement ratio. It can be assumed that the effect of the greater deformation caused by plastic deformation of the main reinforcement may be implicitly considered in the shear capacity formula as,

$$V_c^* = 0.9\beta_p(\rho_{eq}) \cdot \beta_2(f_c') \cdot \beta_d(d) \quad (13)$$

where, ρ_{eq} is the equivalent main reinforcement after yielding and $\rho_{eq} = \rho_{eq}(\mu)$. Then, we have,

$$\frac{V_c^*}{V_c} = \varphi(\mu) \quad (14)$$

Here, the reduced shear carrying capacity at the failure point is described as a function of ductility ratio. From the experiment data, the relationship between loss in shear carrying capacity of concrete and ductility ratio (specimens with shear span-to-depth ratio being equal to 4) is shown in Fig. 32. From this figure, two main tendencies can be recognized. One is that the shear carrying capacity of concrete always falls as the ductility ratio increases. Another is that the relation between ductility ratio and shear carrying capacity of concrete at failure is close to a straight line, as shown in Fig. 32.

The experimental results for different shear span to depth ratio are shown in Fig. 33. It is be found that for specimens with a larger shear span-to-depth ratio, the shear carrying capacity of the concrete falls more than for those with a smaller shear span to depth ratio.

Considering the experimental results shown in Fig. 32 and Fig. 33, a single simple curve-fitting formula is empirically developed for describing the relationship between shear capacity and the ductility ratio as,

$$\frac{V_c^*}{V_c} = (1 - k(\mu - 1)) \quad (15)$$

where, $V_c^* = V_c$ when $\mu < 1$; and $V_c^* = 0$ when $\mu > 1 + 1/k$

$$k = \frac{1}{2(9 - a/d)}$$

From Eq.14 and Eq.15, the ductility ratio of a designed column when shear failure occurs is,

$$\mu = 1 + \frac{1}{k} \left(1 - \frac{P_y - V_s}{V_c}\right) \quad (16)$$

where, $\mu < 1$ when $V_c + V_s < P_y$; $\mu > 1 + 1/k$ when $V_s \geq P_y$. The ranges of application for this formula are shown in Fig.32 and Fig.33.

The predicted ductility ratios of the 53 RC columns are compared with the actual experimental results in Fig. 34. Even through the results are some what scattered, the overall trend means that the ductility ratio can be predicted roughly by this simplified method. The curve drawn here is just for RC columns with no any side reinforcement. For a more versatile prediction, the 3D effects of the presence of side reinforcement should be incorporated in the future. And also in the future, Eq.(16) will be compared with some existing formulas for ductility prediction.

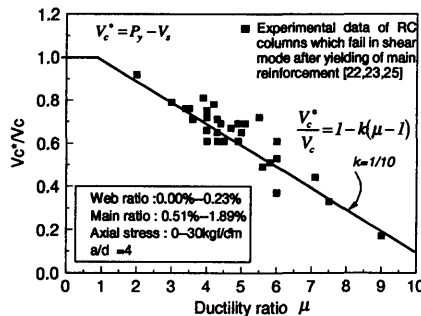


Fig. 32 Relationship between shear carrying capacity of concrete and ductility ratio ($a/d=4$)

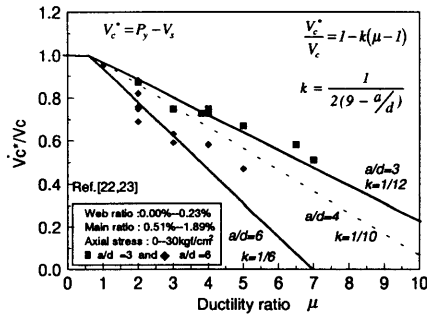


Fig. 33 Effect of a/d on relation between shear carrying capacity of concrete and ductility ratio (a/d=3–6)

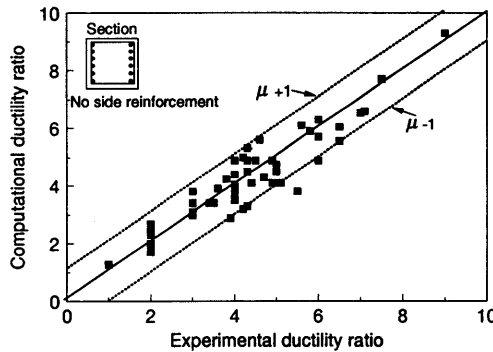


Fig. 34 Computational and experimental ductility ratio

6. CONCLUSIONS

A nonlinear failure analysis based on the spatially averaged constitutive laws for concrete and RC demonstrated that existing large scale RC columns with little web reinforcement tend to fail in shear mode, as the shear capacity is less than the shear load at yield point of the main reinforcement. Seismic-resistant design requires that sufficient shear capacity and ductility is maintained to avoid sudden shear failure and to ensure seismic energy absorption.

Shear failure can occur even after yielding of main reinforcement, because the shear carrying capacity of concrete may fall with plastic deformation of the reinforcement. An FEM code was proposed for simulating the shear failure and ductility of RC columns, and as being in fair agreement with experimental results even for large-scale sections. Since experimental evidence indicates that main reinforcement, web reinforcement ratio, shear span-to-depth ratio, and axial force may affect the ductility of RC columns, FEM was used to examine how rationally the sensitivity of these influences would be predicted.

The FEM code can be used to examine the seismic-resistant performance of structures designed in the past. With the aim of developing a simple method of guidance for the re-design procedure, the relationship between the reduction in shear carrying capacity and ductility ratio at shear failure was evaluated, and a simple formula was proposed for roughly estimate the ductility ratio of RC columns in the design loop.

The simple formula used to describe the decrease in shear carrying capacity of concrete is rather rough, and further research needs to be done to take into account the effects such as the presence of side main reinforcement and axial force.

REFERENCES

- [1] Okamura, H., Maekawa, K., Ozawa, K. and Ohuchi, M.: Damage of concrete bridge piers, *Journal of JSCE*, Vol.80, No.4, pp.11-19, April, 1995 (in Japanese)
- [2] AN, X., Maekawa, K. and Okamura, H.: Numerical simulation of size effect in shear strength of RC beams, *Journal of Materials, Concrete Structures and Pavements*, No.564/V-35, pp297-316, 1997
- [3] Okamura, H. and Maekawa, K.: *Nonlinear Analysis and Constitutive Models of Reinforced Concrete*, Gihodo-Shuppan, Tokyo, Japan, 1991
- [4] Okamura, H. and Maekawa, K.: Reinforced concrete design and size effect in structural nonlinearity, invited paper, *Proceedings of JCI International Workshop on Size Effect*, Sendai, Japan, pp.1-20,1993
- [5] Maekawa, K. and Hasegawa, T.: The state-of-the-art on constitutive laws of concrete, *Concrete Journal*, Vol.32, No.5, pp.13-22, 1994
- [6] Li, B., Maekawa, K. and Okamura, H.: Contact density model for stress transfer across cracks in concrete, *Journal of the Faculty of Engineering, University of Tokyo (B)*, Vol.40, No.1, pp.9-52, 1989
- [7] Tepfers, R.: A theory of bond applied to overlapped tensile reinforcement splices for deformed bars, *Publication 73:2, Division of Concrete Structures, Chalmers University of Technology*, Goteborg, Sweden, 1973
- [8] Jinno, Y. Fujii, S., et al.: Bar size effect on bond characteristics with splitting of surrounding concrete, *Summaries of technical papers of annual meeting, AIJ*, pp747-748, 1986
- [9] Bazant, Z.P. and Oh, B.H.: Crack band theory for fracture of concrete, *Material and Structures*, (RILEM, Paris), Vol.16, pp155-157, 1983
- [10] JSCE, *Standard specification for design and construction of concrete structure*, 1st ed, Tokyo, 1986
- [11] Ohta, M.: A study on earthquake resistant design for reinforced concrete bridge piers of single-column type, *Report of civil research institute*, No.153, March 1980 (in Japanese)
- [12] Ishibashi, T. and Yoshino, S.: Study on deformation capacity of reinforced concrete bridge piers under earthquake, *Journal of JSCE*, No.390/V-8, 1988 (in Japanese)
- [13] JSCE, *Standard specification for seismic resistant design of concrete structure*, 1st ed, Tokyo, 1996
- [14] Kobayashi, N., Kashiwazaki, T. and Noguchi, H.: A study on shear deterioration after flexural yielding of reinforcement concrete beams, *Proc. of JCI*, Vol.17, No.2, pp.571-576, 1995 (in Japanese)
- [15] Higai, T., Niwa, J. and Okamura, Y.: Considerations on the post-yield shear failure mechanism of RC members, *Proc. of JCI*, Vol.8, No.2, pp.329-334, 1987 (in Japanese)
- [16] Muguruma, H. and Watanabe, F.: Effect of yielding in web reinforcement upon the shear deformation capacity of reinforced concrete column, *Proc. of JCI*, Vol.1, pp.333-336, 1979 (in Japanese)
- [17] Muguruma, H. and Watanabe, F.: Strength evaluation of R/C column failing in shear, *Proc. of JCI*, Vol.7, No.2, pp.541-544, 1985 (in Japanese)
- [18] Higai, T., Rizkalla, S. Ben-omran, H. and Saadat, F.: Shear failure of reinforcement members subjected to large deflection reversals, *Proc. of JCI*, Vol.6, pp.505-508, 1984 (in Japanese)
- [19] Higai, T.: Ductility of reinforced concrete members failing in shear due to large deflection reversals, *Proc. of JCI*, Vol.8, pp.769-772, 1986 (in Japanese)
- [20] Arakawa, T. and Fujita, Y.: Effectiveness of shear reinforcement on deformation behavior of reinforced concrete columns subjected to cyclic loading, *Proc. of JCI*, Vol.2, pp.457-460, 1980 (in Japanese)
- [21] Arakawa, T., Arai, Y., Fujita, Y. and Mizoguchi, M.: Evaluation for deformation behavior of reinforced concrete columns under cyclic loading, *Proc. of JCI*, Vol.2, pp.449-452, 1981 (in Japanese)
- [22] Arakawa, T., Arai, Y., Fujita, Y. and Egashira, K.: Effects of cyclic loading rate on the load-carrying capacity and inelastic behavior of reinforced concrete columns, *Proc. of JCI*, Vol.4, pp.325-328, 1982
- [23] Arakawa, T., Arai, Y., Egashira, K. and Ohkubo, S.: Cyclic behavior and evaluation of inelastic capacity of reinforced concrete columns, *Proc. of JCI*, Vol.5, pp.305-308, 1983 (in Japanese)
- [24] Machida, A., Mutsuyoshi, H. and Toyoda, K.: Evaluation of the ductility of reinforced concrete members, *Journal of JSCE*, No.378/V-6, pp.203-212, 1987 (in Japanese)
- [26] Bujadham, B. and Maekawa, K.: The universal model for stress transfer across cracks in concrete, *Proc. of JSCE*, No.451/V-17, pp277-287, 1992